Collector-up light-emitting charge injection transistors in *n*-InGaAs/InAlAs/*p*-InGaAs and *n*-InGaAs/InP/*p*-InGaAs heterostructures

G. L. Belenky, P. A. Garbinski, S. Luryi, M. Mastrapasqua, A. Y. Cho, R. A. Hamm, T. R. Hayes, E. J. Laskowski, D. L. Sivco, and P. R. Smith
AT&T Bell Laboratories, Murray Hill, New Jersey 07974

(Received 23 November 1992; accepted for publication 4 March 1993)

The realization of collector-up light-emitting complementary charge injection transistors is reported. The devices have been implemented in molecular-beam-epitaxy-grown *n*-InGaAs/InAlAs/*p*-InGaAs and *n*-InGaAs/InP/*p*-InGaAs heterostructures using a self-aligned process for the collector stripe definition. Electrons, injected over the wide-gap heterostructure barrier (InAlAs or InP) by the real-space transfer (RST) process, luminesce in the low-doped *p*-type InGaAs active layer. An essential feature of present devices, besides their self-aligned collector-up configuration, is a relatively heavy doping of the *n*-type emitter channel, with the sheet dopant concentration of 4×10^{12} cm^{-2}. This ensures a higher uniformity of the electric field in the channel and provides a relief from RST instabilities at a high level of collector current (linear density $\sim$10 A/cm). Devices with InAlAs and InP barriers show rather different optical characteristics, mainly due to the different band lineups $\Delta E_C/\Delta E_V$ in InGaAs/InAlAs and InGaAs/InP heterostructures, leading to different ratios between the RST current and the parasitic leakage of holes from the collector into the channel. At high RST current densities, the effective carrier temperature T_e in the active collector layer, determined from the high-energy tails of the luminescence spectra, is strongly enhanced compared to the lattice temperature. This decreases the device radiative efficiency and leads to a thermionic emission of carriers out of the active layer.

I. INTRODUCTION

The charge injection transistor[1] (CHINT) is a three-terminal heterojunction device which operates on the principle of real-space transfer (RST) of electrons, heated by a lateral field, over an energy barrier into the adjacent *collector* layer. The heating electric field along the *emitter* channel is provided by "source" and "drain" electrodes. Charge injection transistors have been extensively studied both experimentally[1–10] and theoretically.[11–16]

Most of the experimental investigations dealt with *unipolar* devices (collector contact ohmic for the majority type of carriers in the emitter which are involved in the RST process) and were implemented in a *down-collector* configuration. The latter term means that the collector layer is grown epitaxially prior to the barrier and emitter layers. Implementations of the unipolar down-collector CHINT have been reported in GaAs/AlGaAs,[1,2,8] InGaAs/InAlAs[3,4] and strained-layer InGaAs/AlGaAs/GaAs,[6,7] and GeSi/Si[9] heterosystems. Most of these studies involved *n*-type CHINT, but devices based on the RST of holes have also been reported.[8,9]

All down-collector devices have unavoidable overlaps between the source/drain regions and the collector layer which give rise to parasitic capacitances and limit the microwave performance. The ultimate frequency performance of CHINT is limited by the time of flight of hot electrons over high-field regions of the device, i.e., over distances of order the barrier-layer thickness. The highest cutoff frequencies, reported in a down-collector CHINT structure, were 40 GHz both for the current and the power gain.[4] These results, obtained in a InGaAs/InAlAs heterostructure with a 2000-Å-thick InAlAs barrier, were already limited by the parasitic capacitance, so that a reduction in the barrier thickness would only slow down the device. Although in principle the microwave performance of down-collector CHINT can be further improved by reducing the lateral dimensions of source/drain electrodes, it is clear that collector-up configurations offer significant advantages in that the parasitic capacitances can be effectively eliminated by patterning the collector stripe. The first collector-up CHINT demonstrated[5] a 60 GHz current gain cutoff f_T and a lower (presumably due to the parasitic resistances in a non-self-aligned structure) power-gain cutoff $f_{max}=18$ GHz. With sufficiently narrow barriers, a collector-up CHINT can be expected to outperform the field-effect transistor (FET) of similar geometry [CHINT collector corresponding to field effect transistor (FET) gate] because the small-signal performance of CHINT is not limited by the time of flight between the source and the drain.[1] This advantage was recently demonstrated experimentally[10] by a direct comparison between the microwave performance of the CHINT mode and the FET mode of amplification in the same collector-up device.

Light-emitting charge injection transistors, employing the RST injection of emitter carriers in a collector layer of a complementary conductivity type, were proposed[17] and implemented[18] relatively recently. The potential usefulness of such devices stems from the unique symmetry property[15] of RST transistors, which consists in the fact that the direction of the output (collector) current I_C is the same irrespective of the polarity of the input (heating) voltage. This symmetry, unavailable in other transistors, implies that the output current in CHINT (and the emitted light

 0021-8979/93/128618-10$06.00

in a complementary CHINT) is an exclusive OR function of the voltage signals V_S and V_D applied to the source and drain electrodes: $I_C = \mathrm{XOR}(V_S, V_D)$. Based on this principle, a device with three input source/drain terminals has been proposed[19] in which the collector current is either an OR or a NAND function of any two of the input voltages—with the possibility of switching between these functions by the third input voltage. Similar logic functionality has been predicted[17] for RST light-emitting devices and lasers. Recently, the optoelectronic logic elements XOR and OR-NAND were demonstrated for the first time.[20,21] These devices were implemented in *n*-InGaAs/InAlAs/*p*-InGaAs heterostructures in the down-collector configuration.

The present work reports the first realization of collector-up complementary RST transistors, implemented in both *n*-InGaAs/InAlAs/*p*-InGaAs and *n*-InGaAs/InP/*p*-InGaAs heterostructures. To our knowledge, this is also the first report of a InP-barrier CHINT. An essential feature of our devices is self-alignment of the source/drain contacts to the collector stripe. Another noteworthy element is the use of a heavily doped emitter, which provides a relief from RST instabilities at a high level of collector current. Our collector-up *n*-InGaAs/InAlAs/*p*-InGaAs CHINT shows comparable characteristics, both electric and optical, to collector-down devices with similar structural parameters. However, devices with InP barriers show rather different optical characteristics, mainly due to the different band lineups $\Delta E_C/\Delta E_V$ in InGaAs/InAlAs and InGaAs/InP heterostructures. The band discontinuities ΔE_C and ΔE_V in these heterostructures, as determined by a variety of techniques, have been listed most recently by Yu *et al.*[22] The room-temperature values ($\Delta E_C, \Delta E_V$) appear to converge to (0.5, 0.2) eV in $In_{0.53}Ga_{0.47}As/In_{0.52}Al_{0.48}As$ and (0.25, 0.34) eV in $In_{0.53}Ga_{0.47}As/InP$ heterostructures. These discontinuities are most important in the determination of the leakage currents between the channel and the collector due to thermionic emission of "cold" carriers.

An interesting characteristic of the light-emitting CHINT is its radiative efficiency. In general, it depends on the ratio of the electron RST current to the "parasitic" component of the collector current due to the leakage of holes as well as on the ratio of the radiative and nonradiative recombination rates for electrons injected in the active region and holes in the channel. For InAlAs-barrier devices, the optical logic performance is superior to the electrical logic performance (as measured by the output on/off ratio),[20] because holes injected in the channel undergo mostly nonradiative recombination. For InP-barrier heterostructures, in contrast, the barrier for holes is higher than that for electrons (so that hole current is no longer the dominant component of the parasitic non-RST current, as is the case in InAlAs-barrier devices) and one can expect that the electrical and optical logic on/off ratios should be comparable.

The epitaxial structure and the fabrication sequence, used for both InAlAs and InP barrier devices, are described in Sec. II. Section III presents the results of experimental characterization, both electrical and optical. In addition to the overall measured power P_L of the emitted radiation, we present the *luminescence spectra* at various levels of the collector current. The high-energy tails of these spectra contain information about the effective carrier temperature T_e in the active layer. We find that at high injection currents (linear density ~ 10 A/cm) there is a strong departure of T_e from the ambient temperature T. The enhanced T_e degrades the device radiative efficiency and leads to a thermionic emission of carriers out of the active layer. These issues are discussed in Sec. IV. Section V summarizes our conclusions.

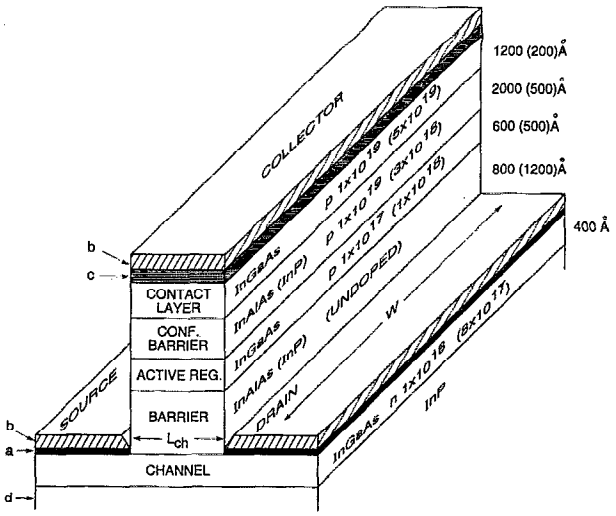

FIG. 1. Schematic diagram of the collector-up complementary charge injection transistor. Letters and numbers in parentheses refer to InP-barrier device. (a) 550 Å Ni/Ge/Au/Ag/Au alloyed channel contact; (b) 2500 Å Si_3N_4 layer; (c) 3000 Å Au collector contact; (d) semi-insulating InP substrate.

II. EPITAXIAL STRUCTURES AND DEVICE FABRICATION

The device structure of collector-up complementary CHINT, obtained after a combination of dry and chemical etchings, is illustrated in Fig. 1. For the sake of economy, both InAlAs and InP-barrier devices are represented, with the parameters of the latter shown in parentheses. All patterns were defined by a standard optical contact lithography.

InAlAs-barrier devices were grown by molecular beam epitaxy (MBE) at 550 °C on a semi-insulating iron-doped InP (100) substrate. Oxide desorption from the substrate occurred at 530 °C. The sequence of epitaxially grown layers was as follows: a 1000 Å undoped $In_{0.52}Al_{0.48}As$ buffer layer, a 400 Å Si-doped (10^{18} cm^{-3}) $In_{0.53}Ga_{0.47}As$ channel, and a 800 Å undoped $In_{0.52}Al_{0.48}As$ barrier, followed by a *p*-type collector structure consisting of a 600 Å Be-doped (10^{17} cm^{-3}) $In_{0.53}Ga_{0.47}As$ active layer and a 2000 Å Be-doped (10^{19} cm^{-3}) $In_{0.52}Al_{0.48}As$ confinement layer, capped with a 1200 Å Be-doped (10^{19} cm^{-3}) $In_{0.53}Ga_{0.47}As$ layer.

The structures were fabricated into devices using optical lithography and selective wet etching. First, a 3000 Å thick Au layer was patterned by lift-off in a dumbbell shape of the collector; this layer was then used as an etch mask. To avoid excessive undercutting, we used a nonselective etch to rapidly etch down to somewhere in the middle of InAlAs barrier layer and then HCl/H_2O to selectively etch the remaining portion of the barrier, stopping at the InGaAs channel layer. A key fabrication step involves the evaporation of the self-aligned source/drain metal which has to provide an ohmic contact without degrading the collector quality and the integrity of the barrier. Needless to say, the metal has to break at the vertical sidewall. The contacts were evaporated using a standard Ni/Ge/Au/Ag/Au sequence—but with a total thickness of only 550 Å—subsequently alloyed at 390 °C for 5–10 s. In the last fabrication step both wafers were blanket covered with a 2500 Å-thick Si_3N_4 layer deposited at 300 °C, then windows were opened and final metal (Au, 2500 Å) evaporated to form contact pads.

The InP barrier structure was grown by metalorganic MBE technique (MOMBE) on a similar substrate at 510 °C. The growth technique has been described in detail previously.[23] Arsine and phosphine served as group V sources, trimethylindium and triethylgallium as group III sources. Thermal beams of Be and Sn, derived from elemental sources, served as *p*-type and *n*-type dopants, respectively. A 300 Å undoped InP buffer layer was followed by a 400-Å-thick $In_{0.53}Ga_{0.47}As$ channel, nominally doped to $N_D=8\times10^{17}$ cm^{-3}, and a 1200-Å-thick InP barrier. Knowing from experience that undoped InP layers come out slightly *n*-type, we have built into the otherwise nominally undoped barrier a 10-Å-thick compensating sheet of acceptors (Be, 3×10^{18} cm^{-3}) located 250 Å away from the channel. The collector layer structure consists of a 500 Å Be-doped (10^{18} cm^{-3}) $In_{0.53}Ga_{0.47}As$ active layer and a 500 Å Be-doped (3×10^{18} cm^{-3}) InP confinement layer, capped with a 200 Å Be-doped (5×10^{19} cm^{-3}) $In_{0.53}Ga_{0.47}As$ layer.

The InP-barrier devices were fabricated using a combination of dry and wet chemical etching. The self-aligned source/drain contacts were obtained in a process similar to that for InAlAs-barrier devices, with a patterned collector metal serving as a mask. Reactive ion etching was used to anisotropically (but nonselectively) etch through the collector layers and partially into the InP barrier layer. By stopping within the barrier, the ion-bombardment damage of the channel was avoided. Dry etching was performed in a PK 1241 plasma tool, using a mixture of methane (12.5%) and hydrogen (7.5%) at the total pressure of 100 mTorr. Optical emission spectroscopy was used to identify ternary and binary layers during the dry etching, allowing a precise termination of the procedure. This technique is based on monitoring variations in the intensity of atomic emission from In atoms excited with a discharge upon removal from the wafer surface. Selective removal of the remaining InP barrier layer to expose the InGaAs channel was done in a solution of HCl and H_3PO_4 mixed in a 1-to-9 volume ratio. The choice of this volume ratio was made to provide vertical sidewalls for mesas parallel to the collector stripe oriented along a [011] direction. This reduced the undercutting of the collector contact while allowing a substantial overetch to ensure a complete removal of InP in the source/drain contact area. Subsequent fabrication of source/drain contacts was identical to that described above for InAlAs-barrier devices.

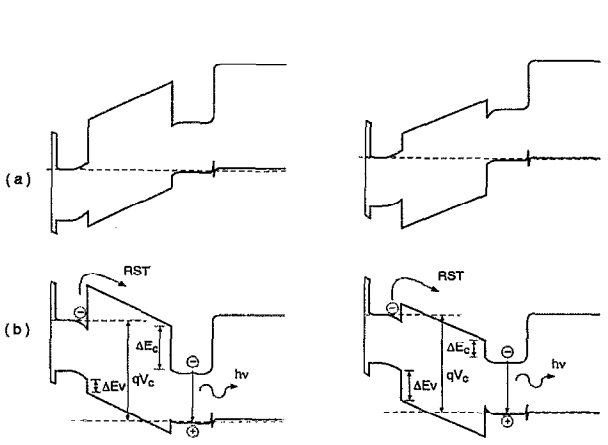

FIG. 2. Band diagram of the device cross section near the source in equilibrium (a) and under positive bias applied to the collector (b). The left half of the figure describes the $In_{0.53}Ga_{0.47}As/In_{0.52}Al_{0.48}As/In_{0.53}Ga_{0.47}As$ heterostructure and the right half the $In_{0.53}Ga_{0.47}As/InP/In_{0.53}Ga_{0.47}As$ heterostructure.

The source-drain separation L_{CH} and the channel width W are defined by the dimensions of the collector stripe. Devices reported in this work have $L_{CH}\times W=1\times20\ \mu m^2$ (InP barrier) and $2\times50\ \mu m^2$ (InAlAs barrier).

III. ELECTRICAL AND OPTICAL CHARACTERIZATION

Results of the characterization are presented in a parallel fashion for InAlAs-barrier devices (Sec. III A) and InP-barrier devices (Sec. III B). It should be noted that while InAlAs-barrier devices can be compared to the collector-down devices, reported previously,[18,20] no such comparison is available for InP-barrier devices. Our own attempts to fabricate a collector-down InP-barrier complementary CHINT have been so far unsuccessful.

Electrical properties of a complementary CHINT are quite different from those of unipolar devices. Most of the differences are rooted in the fact that the collector and the emitter form a *pn* junction with a wide-gap barrier in between. Figure 2 shows the schematic band diagrams in a device cross-section near the source, both at equilibrium and in the operating regime. The device operating regime corresponds to a forward bias of the *pn* junction with the heterostructure barrier being the only impediment to the parasitic flow of cold carriers. The flow of collector holes is blocked by the valence-band discontinuity ΔE_V at the barrier/collector interface and the flow of emitter electrons by the conduction-band discontinuity ΔE_C at the channel/barrier interface.

The luminescence signal was detected from the back of polished samples. To measure the total emitted power P_L we used a broad-area Ge photodiode and suitable focusing

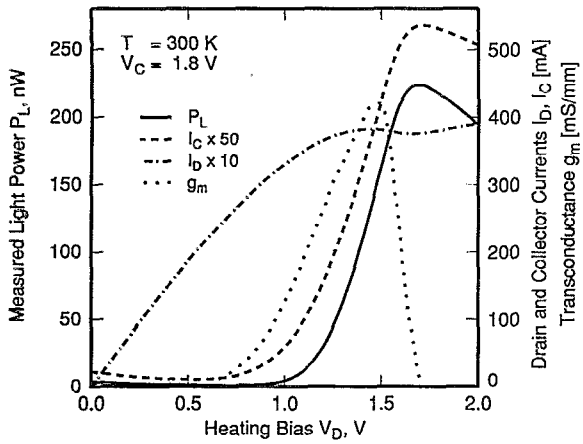

FIG. 3. Room-temperature characteristics of the InAlAs-barrier collector-up complementary CHINT at a constant collector bias V_C=1.8 V.

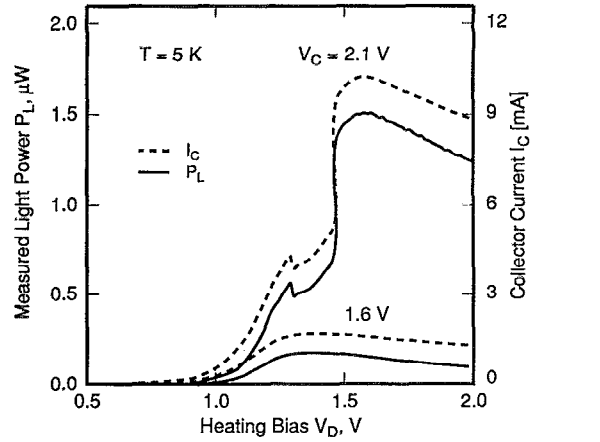

FIG. 4. Cryogenic characteristics of the InAlAs-barrier collector-up complementary CHINT at two collector biases.

optics. From the measured P_L at a given electrical bias configuration, we estimated the internal radiative efficiency of the complementary CHINT as follows:

$$\eta_q = \frac{1}{h\nu \eta_c t_o} \frac{qP_L}{I_C}, \tag{1}$$

where $\eta_c \approx 0.48\%$ is the collection efficiency (estimated assuming that upward directed light is fully reflected from the surface metallization and that the distribution of light intensity is isotropic over the 2π solid-angle hemisphere below the device), $t_o \approx 88\%$ is the combined transmission of the optical components (lens and windows) between the detector and the device, and $h\nu$ is the photon energy at the peak of the luminescence spectrum. The low collection efficiency η_c is accounted for by the total internal reflection, Fresnel loss, and the collection solid angle. We have not used an antireflection coating. The relatively low numerical aperture (NA$\approx$0.34) has been forced by the use of a dewar for low-temperature measurements. Moreover, an error of $\pm 5\%$ in NA from the collection lens being slightly out of focus, produces an error of $\pm 10\%$ in η_c. Nevertheless, the systematic error in the determination of the efficiency was the same for all measurements, since the lens system was not adjusted during the whole set of measurements. The *relative* efficiency behavior of *a given device* at different temperatures and biases can be considered quite reliable. Note that the definition (1) of η_q is different from that used in Ref. 20.

Electroluminescence spectra were registered using a liquid nitrogen cooled Ge detector and a 0.75 m spectrometer. The spectral resolution was better than 1.5 meV.

A. InAlAs barrier devices

Figure 3 shows the characteristics of a 50 μm wide device at 300 K. Electrical behavior of the present device is rather similar to that reported earlier[20] for a collector-down InAlAs-barrier CHINT. As the drain bias is increased from V_D=0, the collector current first decreases (since the collector-emitter voltage, which controls the leakage current, decreases in the channel cross sections near the drain) and then increases when the heating bias becomes sufficiently large ($V_D \gtrsim 1V$) for the RST to begin. At the same time a small negative differential resistance (NDR) appears in the $I_D(V_D)$ characteristic. The decrease in I_D does not fully compensate for the increase in I_C which implies that the source current I_S increases too.

The stippled line in Fig. 3 indicates the transconductance defined by the following expression:

$$g_m \equiv \frac{1}{W}\left(\frac{\partial I_C}{\partial V_D}\right)_{V_C=\text{const}}. \tag{2}$$

At room temperature and fixed collector bias V_C=1.8 V, the transconductance peaks at $g_m \approx 400$ mS/mm near V_D =1.5 V. The existence of a maximum g_m is common to all CHINTs and reflects the tendency of I_C to saturate with increasing heating bias at a given V_C (similar to the saturation of the anode current in a vacuum diode with increasing cathode temperature and fixed anode voltage). At still higher $V_D \approx 1.65$ V, the collector current itself peaks and then decreases. This indicates that most of the RST occurs near the drain where the heating field is highest. High values of V_D cause a reversal of the transverse field so that the effective barrier height near the drain increases, suppressing the RST. For a given bias configuration (V_C,V_D) we find that the RST current increases with the temperature, cf. Fig. 5.

The measured light power P_L increases in proportion to I_C. This behavior is characteristic of InAlAs-barrier devices at all temperatures down to 5 K (Fig. 4), including the regime of a pronounced NDR.

The radiative quantum efficiency (1) is plotted in Fig. 5 as a function of the heating bias for two ambient temperatures and several values of V_C. The dependence $\eta_q(V_D)$ consists of two parts. At low heating biases (prior to the onset of an efficient RST)—where the leakage current decreases with V_D—the efficiency decreases also. This dependence is clearly evident in the room-temperature characteristics, Fig. 5(a); at cryogenic temperatures the

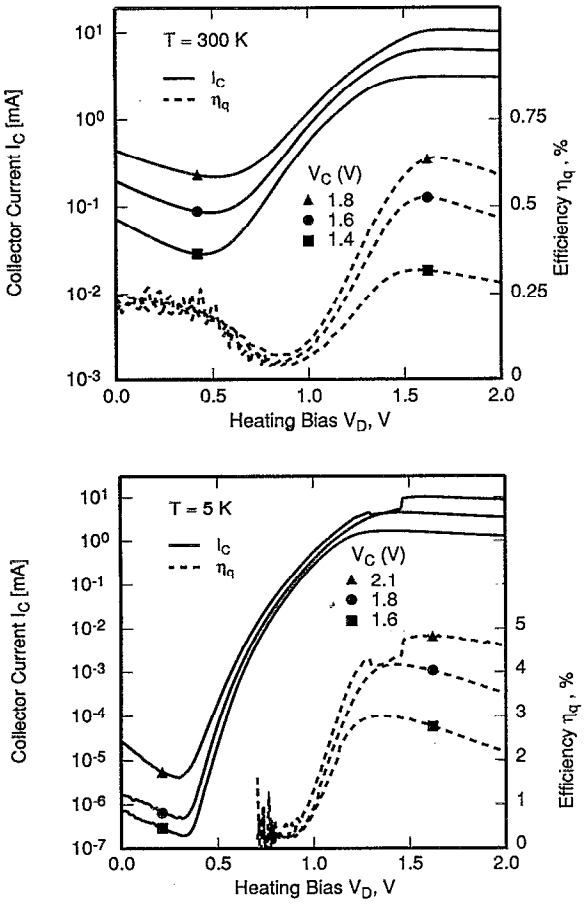

FIG. 5. The dependence of the radiative efficiency, defined by Eq. (1), on the heating bias V_D for several collector biases V_C in InAlAs barrier devices. (a) 300 K; (b) 5 K.

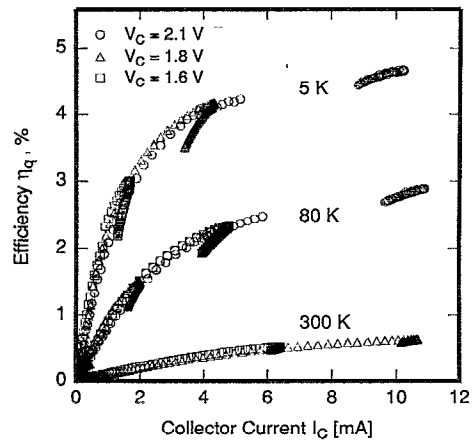

FIG. 6. Correlation between the efficiency η_q and the measured I_C in InAlAs barrier devices for different bias conditions and ambient temperatures. Different curve segments correspond to different fixed values of the collector voltage $V_C(V)$ at which I_C was varied by changing the heating bias V_D.

leakage is so low that its efficiency could not be determined. At higher V_D the efficiency increases with increasing RST.

The efficiency behavior in the leakage region (low V_D) is qualitatively similar to that of the collector-down InAlAs-barrier devices, reported earlier.[20] There is some difference, related to a substantially lower internal radiative efficiency of electrons in the collector active region. This is a consequence of our using a very heavily doped collector confinement barrier. In the experiments[21] with down-collector complementary CHINT it has been ascertained that lowering the doping from 10^{19} to 10^{18} cm^{-3} in a 1000-Å-thick sublayer of the confinement barrier, immediately adjacent to the active region, enhances the internal efficiency of RST electrons by more than an order of magnitude. The other reason for a different behavior originates from the collector-up nature of the present device. In the collector-down device[20] holes injected in the channel have a negligible radiation efficiency, because (a) most of the hole leakage occurs in the wide area under the source/drain contacts and (b) holes injected in the channel recombine nonradiatively at the trench surface or the heavily doped cap layer. In contrast, holes, injected in the n-doped channel of our collector-up device at $V_D=0$, have a relatively high probability of radiative recombination. The characteristic time to reach the contact area by lateral diffusion $L_{CH}^2/4D \gtrsim 10^{-10}$ ps is comparable to the radiative recombination time in the channel. The higher radiative efficiency of holes, combined with lower radiative efficiency of electrons, results in the overall η_q at $V_D=0$ being comparable (within a factor of 3) to the value of η_q at high V_D, where it is dominated by the recombination of RST electrons. We explain the initial decrease of η_q in the low V_D region by the gradual replacement of the relatively slow diffusion process by the faster drift of injected holes to the source contact area.

For $V_D \gtrsim 1.0$ V the collector current is dominated by RST. In Fig. 6 the efficiency is plotted as a function of the current I_C for different biasing conditions at three different temperatures. It is interesting to note that η_q depends on both the temperature and the injection current but not on the collector bias V_C at which a particular value of I_C is reached. The general trend of monotonically increasing $\eta_q(I_C)$ for a given V_C should be attributed to a competition between the radiative and nonradiative recombination processes in the collector active region. [Because of the relatively small difference between the radiative efficiencies of electrons in the active region and holes in the emitter channel (only a factor of ~ 3 in our present devices), the monotonically increasing $\eta_q(I_C)$ cannot be explained by a progressively increasing RST component of I_C.] Indeed, consider the behavior of $\eta_q(I_C)$ at different temperatures in Fig. 6. The low temperature data show a sharp rise of the efficiency at low I_C, followed by a slower growth at higher I_C with a tendency to saturate. At the carrier temperatures $T_e \lesssim 77$ K the interband Auger processes are negligible[24] and the nonradiative recombination in the collector is likely to be dominated by impurity traps at the confinement barrier interface with the active layer and perhaps those in the active layer itself. The nonradiative recombination current is thus proportional to the first power of the electron concentration n injected in the active layer ($\propto A_{nr} n$) and at high values of n its role diminishes relative

to the radiative component ($\propto Bnp$). Here $p=p_0+n$, where p_0 is the equilibrium hole concentration in the active layer. The quantity A_{nr} is the inverse of the nonradiative lifetime in the presence of traps and $B=B(n)$ is the radiative recombination coefficient.[24] The internal efficiency in the collector active layer at low temperatures (where we can neglect the leakage of holes) is thus given by

$$\eta_q=\left(1+\frac{A_{nr}}{Bp}\right)^{-1}, \tag{3}$$

which accounts for the initial sharp rise of η_q in the region $I_C \lesssim 2$ mA at low temperatures. In this regime, one has $p_0 \ll n \lesssim A_{nr}/B$, whence $\eta_q \approx (B/A_{nr})n \propto (B/A_{nr}^2)I_C$. Since A_{nr} increases with the thermal velocity of minority electrons, we can expect a lower slope of $\eta_q(I_C)$ at higher T, in accordance with Fig. 6. As will be shown below, at higher injection currents the carrier temperature strongly departs from the ambient value, $T_e \gg T$, and the behavior of η_q becomes complicated even within the framework of Eq. (3). Moreover, at high T_e one can expect a strong enhancement of the Auger processes, which limits the efficiency rise with I_C and may even lead to a decreasing $\eta_q(I_C)$ at sufficiently high injection levels.

For $T=300$ K one has $p_0 \approx N_A$ (where $N_A=10^{17}$ cm^{-3} is the acceptor concentration in the active layer) and the hole concentration $p=p_0+n$ has relatively weak dependence on the injection current. At the same time, due to the higher thermal velocity of injected electrons, their nonradiative recombination at the interface with the heavily doped confinement barrier is substantially enhanced compared to the situation at cryogenic temperatures. Moreover, at 300 K the efficiency may be affected by Auger processes. As a result, the radiative efficiency is relatively low and has a slower dependence on the collector current.

Note that each curve in Fig. 6 includes the data from different biasing configurations. Each sequence of points, corresponding to a given V_C, ends with a "dangling tail" at high injection currents. This means that after the peak of I_C the efficiency decreases faster than the current, an unambiguous observation which we have not been able to explain consistently.

Figure 7 presents the electroluminescence spectra taken at 5 K and normalized to the same value at the peak. The general shape of these spectra at low I_C is similar to those reported in the literature[25] for the luminescence of electrons and holes photoexcited in InGaAs. The energy position of the peak shifts to higher energies with increasing collector current, which corresponds to increasing injected carrier concentration. At the same time, we see the appearance of a high energy tail, which expands with I_C. Such a transformation of the luminescence spectra is usually observed when the interband optical excitation intensity is increased.[26] The evident linearity of the tail on the semilog plot implies that the carrier distribution at high energies is approximately Maxwellian and can be characterized by an effective temperature T_e. Assuming a fast thermalization between electrons and holes, we can interpret the T_e as a common temperature of the electron-hole plasma in the active layer. The effective temperature, determined from the slope of the high-energy tail, is plotted in Fig. 8 against the collector current. We note that the dependence is approximately linear at high currents but does not extrapolate to $T_e=T$ for $I_C \to 0$. This implies a nonlinear behavior of $T_e(I_C)$ at low levels of injection.

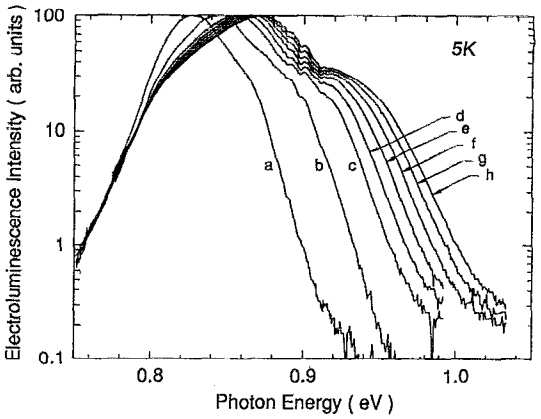

FIG. 7. Normalized electroluminescence spectra in InAlAs barrier devices at 5 K. The spectra were taken under the bias conditions with the following values of I_C (mA): (a) 3.4, (b) 8.3, (c) 10.2, (d) 15.0, (e) 17.7, (f) 20.4, (g) 23, (h) 25.8.

Even higher carrier overheating is observed in room-temperature spectra. However, because of the low η_q at 300 K these spectra are too noisy in the tails for a quantitative interpretation. Nevertheless, for the biasing conditions, corresponding to the data in Fig. 3 in the high RST region, we can safely assert that the carrier temperature is in the range $450 \lesssim T_e \lesssim 550$ K. At such temperatures, the thermionic emission of holes from the active layer into the emitter becomes an important contribution into the transistor current balance. We remark that the thermionic current of holes, stimulated by the carrier overheating, appears indistinguishable from RST in the collector current characteristics. In this

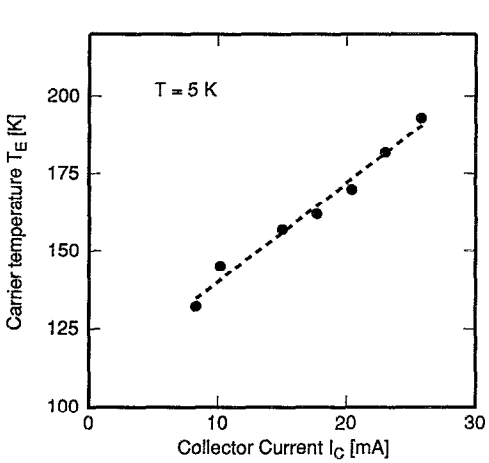

FIG. 8. Effective temperature of the electron-hole plasma in InAlAs barrier devices at 5 K, determined from the slope of high-energy tails in Fig. 7(b). Dashed line represents a linear interpolation. The collector area $A=10^{-6}$ cm^2.

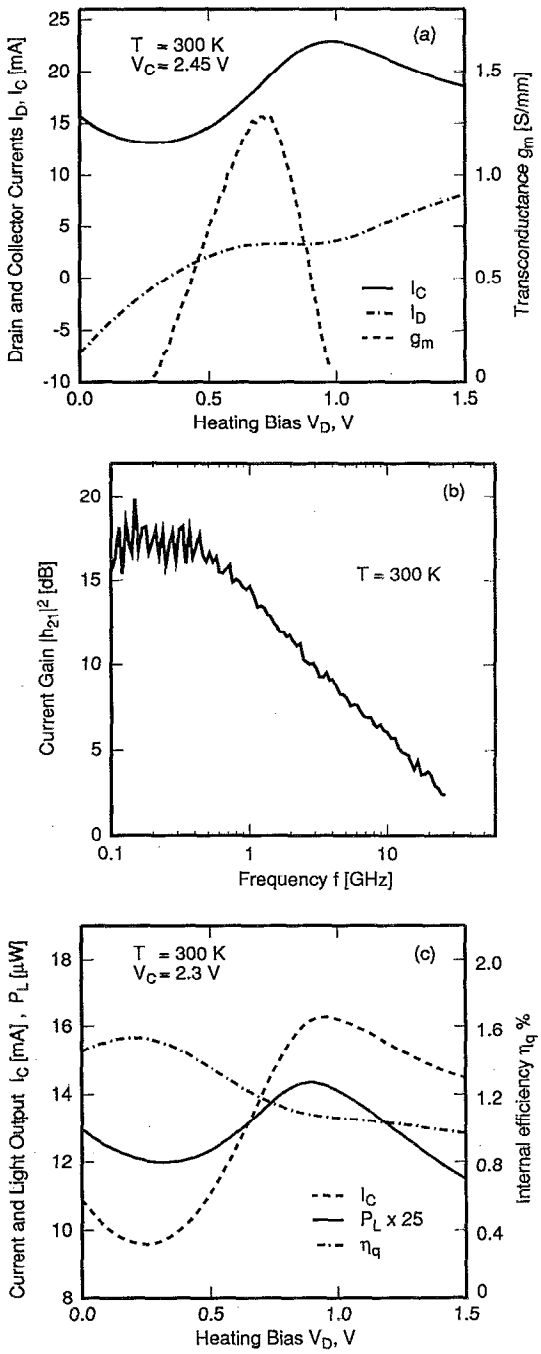

FIG. 9. Room-temperature characteristics of InP-barrier devices. (a) electrical (I_D, I_C, and g_m at a constant V_C=2.45 V and varying V_D); (b) microwave [$|h_{21}|^2(f)$ at fixed V_C=1.97 V and V_D=0.76 V]; (c) optical (P_L, I_C, η_q at a constant V_C=2.3 V and varying V_D).

situation, the apparent radiative efficiency, determined by Eq. (1), will be *lower* than its intrinsic value.

B. InP barrier devices

Room-temperature characteristics of a 20 μm wide device are shown in Figs. 9(a)–9(c). Electrical characterization is presented in Fig. 9(a). At a relatively low collector bias V_C=2.45 eV the RST begins at $V_D \approx 0.5$ V and I_C reaches its maximum at $V_D \approx 1$ V, decreasing at higher heating biases. Large RST injection occurs in the absence of a significant NDR. Similar to the InAlAs-barrier results (Fig. 3) this implies that the RST is accompanied by an increase in the source current I_S. The device transconductance g_m reaches the value of about 1.2 S/mm, which is more than twice that obtained for InAlAs-barrier devices with about twice longer L_{CH}. The high value of g_m in a collector-up device is encouraging from the standpoint of high-speed performance.

Our preliminary microwave measurements, Fig. 9(b), show virtually no decrease in the common-source current gain $|h_{21}|^2$ with the frequency f up to $f \approx 0.5$ GHz. At higher frequencies the gain rolls off at about 8 dB/dec rather than 20 dB/dec normally observed in bipolar transistors. The device still has a $\sim$3 dB gain at 22 GHz, near the highest frequency of our present measurements. Slow gain rolloff has been noted before[4] in unipolar down-collector charge injection transistors. This effect certainly deserves further study, both experimental and theoretical.

Electroluminescence characteristics are shown in Fig. 9(c). A distinctive feature of our InP barrier devices is the fact that their radiative efficiency decreases as a function of the injection current. This trend is observed at all temperatures and is opposite to that noted for InAlAs devices (cf. Fig. 6). The difference is explained by the fact that the surface recombination at the confinement-layer boundary, which was the dominant nonradiative recombination component in our InAlAs-barrier devices, is relatively insignificant in the present InP-barrier devices, where the confinement layer is not as heavily doped. Consequently, we do not see in these devices the efficiency rise, according to the mechanism described by Eq. (3). We believe the decrease in η_q with increasing I_C should be attributed to the increase of the effective carrier temperature in the active layer.

Figures 10(a) and 10(b) show the correlation between the measured values of the efficiency and the collector current at three different temperatures. We note a strong temperature dependence of η_q, as the sample is cooled from 300 K [Fig. 10(a)] to cryogenic temperatures [Fig. 10(b)]. Both the temperature dependence and the current dependence of η_q weaken for higher currents.

Figure 11 shows the electroluminescence spectra of InP barrier devices at the ambient temperature 300 K. The line shape and its spectral position correspond to the photoexcitation data reported in the literature[25] for InGaAs at T=300 K. The semilogarithmic plot clearly shows the exponential high-energy tails which grow with increasing current. The carrier temperature T_e, estimated from these tails, grows from 440 to 570 K.

Similar observation can be made from the cryogenic luminescence spectra, shown in Fig. 12. The carrier temperature T_e, estimated from the high-energy tails, grows from 110 to 255 K. We note that these tails cannot be associated with an enhancement of the lattice temperature. If the measured T_e were to represent the lattice temperature, the band gap would have shrunk by about 50 meV (from the known[27] temperature coefficient $\approx -3.5 \times 10^{-4}$ eV/deg of InGaAs). No evidence of such a change can be seen in the low-energy part of the spectra.

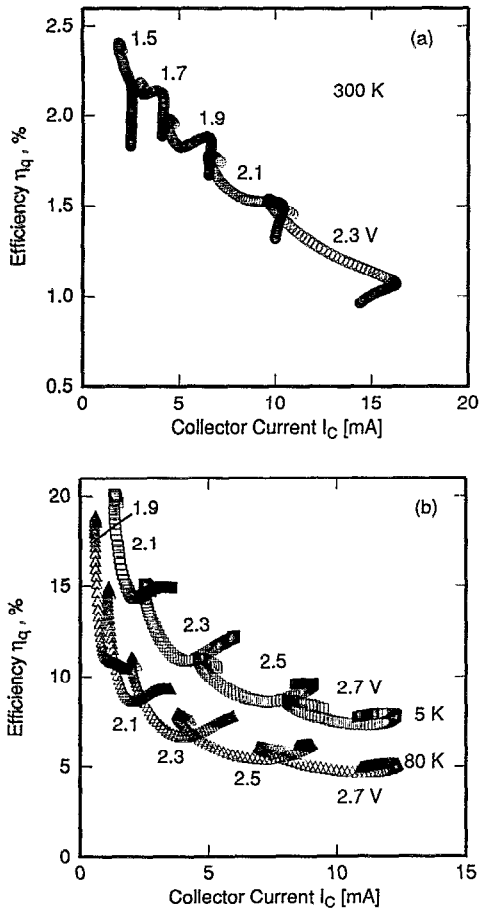

FIG. 10. Correlation of the radiative efficiency of InP barrier devices with the measured collector current. Different curves are labeled by the collector voltage $V_C(V)$ at which I_C was varied with the help of the heating bias V_D. (a) Room temperature, (b) cryogenic temperatures.

The spectra in Fig. 12 show the blue shift of the luminescence peak with higher injection current. The lowest-current spectra are likely to be associated with optical transitions to the acceptor level. However, the position of line *a* in Fig. 12 agrees rather poorly with the literature

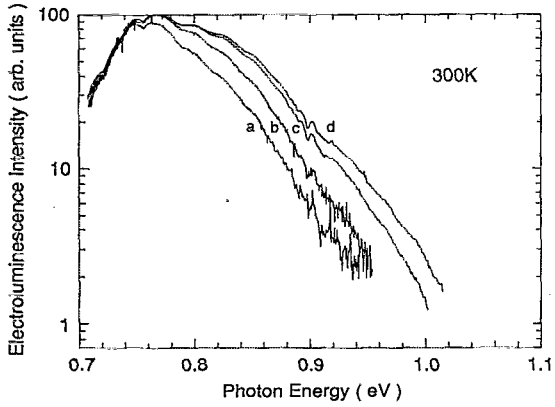

FIG. 11. Room-temperature electroluminescence spectra of InP barrier devices on a semilogarithmic scale. The spectra were taken under the bias conditions with the following values of I_C (mA): (a) 2.5, (b) 4.1, (c) 10.5, (d) 16.3.

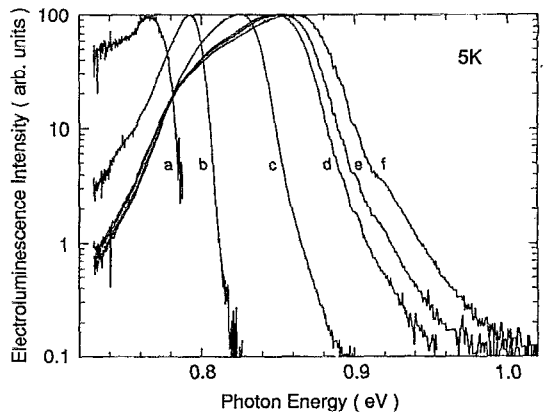

FIG. 12. Normalized electroluminescence spectra of InP barrier devices at 5 K, taken at the following values of I_C (mA): (a) 0.027, (b) 0.132, (c) 1.7, (d) 5.8, (e) 8.8, (f) 12.0.

data[25,28] on the 5 K band gap of InGaAs (E_G=0.804 eV) and the activation energy of Be (E_A=12 meV). The concentration of Be in the active region of our InP-barrier devices is 10^{18}cm^{-3}. At higher injection currents we see a transition to the band-to-band luminescence and the blue shift of the peak corresponds to the band filling effect. The overall shift of about 70 meV between curves *b* and *f* corresponds to $n \approx 6\times 10^{17}\text{cm}^{-3}$.

The effective carrier temperature T_e, determined from the high-energy tails of the luminescence spectra in Figs. 11 and 12, is shown in Fig. 13. We see that the amount of overheating $\Delta T_e \equiv T_e - T$ rises with the injection current. This rise is responsible for the decrease in the efficiency η_q with I_C seen in Figs. 9(c) and 10. The behavior of ΔT_e is qualitatively similar to that seen for InAlAs-barrier devices (cf. Fig. 8), plotted on the same graph; however the attendant decrease of η_q in those devices is masked by the opposite trend, Eq. (3). The overheating ΔT_e is a faster rising function of the injection carrier density at lower tempera-

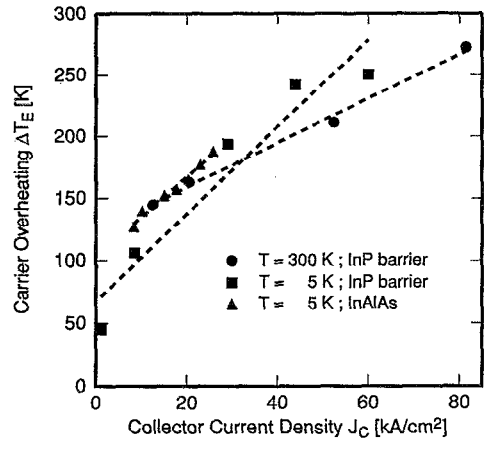

FIG. 13. Effective temperature of carriers, determined from the slope of high-energy tails in Figs. 7(b), 11, and 12(b). The amount of overheating $\Delta T \equiv T_e - T$ is plotted against the injection carrier density per unit area A of the collector. Dashed lines represent linear interpolations. For InAlAs devices $A=10^{-6}$ cm^2 and for InP devices $A=2\times 10^{-7}$ cm^2.

tures. Because of the much higher radiative efficiency in InP-barrier devices, their low temperature spectra permit an estimate of T_e down to lower currents.

IV. DISCUSSION

The key novel constructive feature of the complementary charge injection transistors described in the present work (besides their self-aligned up-collector structure), is the use of a heavily doped emitter channel. The high electron concentration in the channel has led to record magnitudes of the RST current in the bias regime free of NDR instabilities. The collector current density at room temperature reaches 10 and 100 kA/cm^2, respectively, in devices with InAlAs (Fig. 3) and InP [Fig. 9(a)] barriers. In the latter case, at moderate collector biases $V_C \approx 2$ V and in a range of heating biases $0.55 \lesssim V_D \lesssim 0.85$ V, the transconductance g_m exceeds 1 S/mm. Inasmuch as the CHINT transconductance is determined in large measure by the transport of injected charge across the barrier,[1] its microwave performance is expected to be enhanced by the superior[29] hot-electron transport properties of InP. At the same time, the relatively low injection barrier $\Delta E_C \approx 0.25$ eV in the InGaAs/InP system—compared to the satellite-valley separation of 0.55 eV in InGaAs—should suppress the unwelcome intervalley transfer, that often slows down the RST process.[14] The high g_m, together with our preliminary microwave testing results, indicate that up-collector InP-barrier CHINT devices may become useful as high frequency amplifiers.

The obtained high values of the RST current allowed us to investigate the luminescence spectra in a wide range of electron injection levels. The discovered high-energy tails of the luminescence spectra permitted a direct measurement of the carrier temperature T_e in the active collector layer. These studies demonstrate a strong (up to 270 K) overheating of the electron-hole plasma which limits the radiative efficiency in the active layer. Let us briefly discuss the possible origin of the overheating effect as well as its consequences for the electrical and optical properties of the complementary CHINT.

What is the source of heating in the active layer? We can identify at least two mechanisms. The heating power may be partially due to the hot electrons that plunge into the active layer from the barrier. The power dissipated by injected electrons is at least $W_H \gtrsim I_C^{(e)} \Delta E_C / e$, where $I_C^{(e)}$ is the electron component of the collector current. Due to the intercarrier interaction, whose characteristic time at concentrations 10^{18} cm^{-3} is much less than 1 ps,[30] the electron-hole plasma retains a Maxwellian distribution but at an elevated temperature T_e.

At low values of T_e the injected electron power is the only source of carrier heating in the active layer. However, as the carrier temperature increases beyond 200 K, the Auger recombination becomes a tangible component of the total current, whose significance increases with both T_e and I_C. Indeed, each act of an interband Auger transition releases an energy of the order of the band gap $E_G \approx 0.75$ eV into the electron-hole plasma. Denoting by ξ_A the fraction of recombination acts in the collector that go via Auger mechanism, we can estimate the resultant heating power as $W_A \gtrsim \xi_A I_C^{(e)} E_G / e$.

The rise in the carrier temperature T_e can then be estimated from an energy balance equation. Noting that at high carrier concentrations the energy relaxation time in InGaAs can be rather long (several picoseconds[31,32]) due to hot phonon effects, the effective temperature increments ~ 200 K (at $T = 6$ K) and ~ 270 K (at $T = 300$ K), found in our study, appear quite reasonable. Similar magnitudes of overheating have been found in optical excitation experiments[33,34] in $In_{0.53}Ga_{0.47}As$ quantum wells.

The enhanced temperature T_e of electrons and holes in the collector active layer may have important consequences for the electrical characteristics of the complementary CHINT. Depending on the direction of the electric field in the barrier at a given point, either electrons or holes may undergo a thermionic emission from the collector active layer into the emitter. Moreover, in a bias configuration when $0 < V_C - V_{fb} < V_D$, where V_{fb} is the flatband collector bias, *both* components of the overheated plasma may flow into the channel, holes into the region near the source and electrons into the region near the drain electrodes. These secondary fluxes, stimulated by the carrier overheating due to the primary RST flux, form what may be termed the "inverse real-space transfer" process.

V. CONCLUSIONS

Results of the present work may be summarized as follows.

(1) Collector-up complementary CHINT devices have been implemented, in InP-based heterostructure materials, using a self-aligned process for the collector stripe definition. Both the *n*-type emitter channel and the *p*-type collector active region have been implemented as $In_{0.53}Ga_{0.47}As$ layers separated by a wide-gap heterostructure barrier. Both $In_{0.52}Al_{0.48}As$ and InP barrier devices have been investigated.

(2) InAlAs-barrier devices showed a qualitatively similar behavior to that observed previously in down-collector devices of similar heterostructure design. However, our use of a relatively heavy emitter doping resulted in larger injection currents in the regime free of NDR instabilities. Heavy emitter doping levels, in the range 10^{18} cm^{-3}, are promising for optoelectronic applications of the CHINT.

(3) InP-barrier charge injection transistors are reported. Devices of this type, both unipolar and complementary, are promising from the standpoint of microwave performance, due to the high electron velocities in InP. Preliminary microwave testing of our up-collector InP-barrier CHINT's produced encouraging results.

(4) High levels of the collector current density (up to 100 kA/cm^2) obtained in this work permitted a determination of the effective temperature T_e of the electron-hole plasma in the active collector region from the high-energy tails of electroluminescence spectra. We found a significant overheating (by 200–300 K) of carriers and discussed the origin and the implications of this effect.

ACKNOWLEDGMENT

The authors would like to thank T. R. Fullowan for silicon nitride deposition.

[1] S. Luryi, A. Kastalsky, A. C. Gossard, and R. H. Hendel, IEEE Trans. Electron Devices **ED-31**, 832 (1984).
[2] A. Kastalsky, J. H. Abeles, R. Bhat, W. K. Chan, and M. Koza, Appl. Phys. Lett. **48**, 71 (1986).
[3] P. M. Mensz, S. Luryi, A. Y. Cho, D. L. Sivco, and F. Ren, Appl. Phys. Lett. **56**, 2563 (1990); *ibid.* **57**, 2558 (1990).
[4] P. M. Mensz, H. Schumacher, P. A. Garbinski, A. Y. Cho, D. L. Sivco, and S. Luryi, IEDM Tech. Dig. **1990**, 323.
[5] M. R. Hueschen, N. Moll, and A. Fischer-Colbrie, Appl. Phys. Lett. **57**, 386 (1990).
[6] M. E. Favaro, G. E. Fernández, T. K. Higman, P. K. York, L. M. Miller, and J. J. Coleman, J. Appl. Phys. **65**, 378 (1989).
[7] M. E. Favaro, J. J. Alwan, R. P. Bryan, L. M. Miller, J. J. Coleman, J. Kim, and C. M. Wayman, Electron. Lett. **26**, 1264 (1990).
[8] M. E. Favaro, L. M. Miller, R. P. Bryan, J. J. Alwan, and J. J. Coleman, Appl. Phys. Lett. **56**, 1058 (1990).
[9] P. M. Mensz, S. Luryi, J. C. Bean, and C. J. Buescher, Appl. Phys. Lett. **56**, 2663 (1990).
[10] K. Maezawa and T. Mizutani, Jpn. J. Appl. Phys. **30**, 1190 (1991).
[11] A. A. Grinberg, A. Kastalsky, and S. Luryi, IEEE Trans. Electron Devices **ED-34**, 409 (1987).
[12] I. C. Kizilyalli, K. Hess, T. Higman, M. Emanuel, and J. J. Coleman, Solid-State Electron. **31**, 355 (1988).
[13] M. Mouis, F. Paviet-Salomon, P. Dollfus, and R. Castagné, J. Phys. (Paris) Colloq. **49**, 567 (1988).
[14] I. C. Kizillyalli and K. Hess, J. Appl. Phys. **65**, 2005 (1989).
[15] S. Luryi and M. R. Pinto, Phys. Rev. Lett. **67**, 2351 (1991); Semicond. Sci. Technol. **7**, B520 (1992).
[16] M. R. Pinto and S. Luryi, IEDM Tech. Dig. **1991**, 507.
[17] S. Luryi, Appl. Phys. Lett. **58**, 1727 (1991).
[18] M. Mastrapasqua, F. Capasso, S. Luryi, A. L. Hutchinson, D. L. Sivco, and A. Y. Cho, Appl. Phys. Lett. **60**, 2415 (1992).
[19] S. Luryi, P. M. Mensz, M. R. Pinto, P. A. Garbinski, A. Y. Cho, and D. L. Sivco, Appl. Phys. Lett. **57**, 1787 (1990).
[20] M. Mastrapasqua, S. Luryi, F. Capasso, A. L. Hutchinson, D. L. Sivco, and A. Y. Cho, IEEE Trans. Electron Devices **ED-40**, 250 (1993).
[21] M. Mastrapasqua, S. Luryi, G. L. Belenky, P. A. Garbinski, D. L. Sivco, and A. Y. Cho, IEDM Tech. Dig. **1992**, 659; IEEE Trans. Electron Devices (to be published).
[22] E. T. Yu, J. O. McCaldin, and T. C. McGill, in Solid State Physics, edited by H. Ehrenreich and D. Turnbull (Academic, Boston, 1992), Vol. 46, pp. 41–49.
[23] D. Ritter, R. A. Hamm, A. Feygenson, M. B. Panish, and S. Chandrasekhar, Appl. Phys. Lett. **59**, 3431 (1991).
[24] G. P. Agrawal and N. K. Dutta, *Long-wavelength Semiconductor Lasers* (Van Nostrand Reinhold, New York, 1986).
[25] I. C. Bassignana, C. J. Miner, and N. Puetz, J. Appl. Phys. **65**, 4299 (1989).
[26] K. Leo, W. W. Rühle, and K. Ploog, Phys. Rev. B **38**, 1947 (1988).
[27] N. K. Dutta and R. J. Nelson, IEEE J. Quantum Electron. **QE-18**, 44 (1982); S. Adachi, J. Appl. Phys. **53**, 8775 (1982).
[28] Y.-H. Zhang, R. Cingolani, and K. Ploog, Phys. Rev. B **44**, 5958 (1991).
[29] M. A. Littlejohn, J. R. Hauser, T. H. Glisson, D. K. Ferry, and J. W. Harrison, Solid-State Electron. **21**, 107 (1978).
[30] R. A. Höpfel, J. Shah, P. A. Wolf, and A. C. Gossard, Phys. Rev. B **37**, 6941 (1988).
[31] D. J. Westland, J. F. Ryan, M. D. Scott, J. I. Davies, and J. R. Riffat, Solid-State Electron. **31**, 431 (1988).
[32] H. Lobentanzer, W. Stolz, K. Ploog, R. J. Bäuerle, and T. Elsaesser, Solid-State Electron. **32**, 1875 (1989).
[33] H. Lobentanzer, W. W. Rühle, H.-J. Polland, W. Stolz, and K. Ploog, Phys. Rev. B **36**, 2594 (1987).
[34] U. Cebulla, A. Forchel, G. Bacher, D. Grützmacher, W. T. Tsang, and M. Razeghi, Solid-State Electron. **32**, 1669 (1989).